Biosynthesis of *O*-*N*-acetylgalactosamine glycans in the human cell nucleus

Received for publication, August 23, 2018, and in revised form, December 20, 2018 Published, Papers in Press, December 27, 2018, DOI 10.1074/jbc.RA118.005524

Romina B. Cejas, Virginia Lorenz[1], Yohana C. Garay, and Fernando J. Irazoqui[2]

From the Centro de Investigaciones en Química Biológica de Córdoba, CIQUIBIC, CONICET, and Departamento de Química Biológica Ranwel Caputto, Facultad de Ciencias Químicas, Universidad Nacional de Córdoba, Ciudad Universitaria, X5000HUA Córdoba, Argentina

Edited by Gerald W. Hart

Biological functions of nuclear proteins are regulated by post-translational modifications (PTMs) that modulate gene expression and cellular physiology. However, the role of *O*-linked glycosylation (*O*-GalNAc) as a PTM of nuclear proteins in the human cell has not been previously reported. Here, we examined in detail the initiation of *O*-GalNAc glycan biosynthesis, representing a novel PTM of nuclear proteins in the nucleus of human cells, with an emphasis on HeLa cells. Using soluble nuclear fractions from purified nuclei, enzymatic assays, fluorescence microscopy, affinity chromatography, MS, and FRET analyses, we identified all factors required for biosynthesis of *O*-GalNAc glycans in nuclei: the donor substrate (UDP-GalNAc), nuclear polypeptide GalNAc -transferase activity, and a GalNAc transferase (polypeptide GalNAc-T3). Moreover, we identified *O*-GalNAc glycosylated proteins in the nucleus and present solid evidence for *O*-GalNAc glycan synthesis in this organelle. The demonstration of *O*-GalNAc glycosylation of nuclear proteins in mammalian cells reported here has important implications for cell and chemical biology.

The nucleus is one of the most important structures of eukaryotic cells. This complex organelle stores the chromosomes and also regulates their duplication, segregation, repair, and expression through a series of specific processes. The cell's biological information is saved and transferred within the nucleus by three types of biopolymer molecules: DNA, RNA, and proteins (1). Proteins play crucial roles in nuclear scaffolding, DNA assembly, replication, transcription, and transport of molecules. The biological activity of proteins is directly modulated by their conformation, and changes in protein conformation are controlled mainly by post-translational modifications (PTMs).[3] The common PTMs of nuclear proteins are acetylation, sumoylation, phosphorylation, long-chain fatty acid conjugation, and glycosylation. A given PTM adds a tag to proteins that can be recognized by specific molecules (*e.g.* bromodomain for acetyl residue; lectin for glycan) as a trigger of biological effect (2, 3). Thus, biological functions of nuclear proteins can be regulated via PTMs. PTMs of nuclear proteins play a central role in epigenetic physiology, *i.e.* modulation by environmental factors of cellular phenotype other than by the effects of genetic encoding of information.

Glycosylation is the most common PTM of proteins; >50% of cellular proteins are potential targets of glycosylation. Protein *O*-GlcNAc glycosylation (biosynthesis of *O*-GlcNAc glycans) occurs in the nucleus, cytoplasm, and mitochondria (4). *O*-GlcNAc is added by multiple alternatively spliced isoforms of the enzyme GlcNAc transferase (OGT), which have different intracellular localizations (5). There are three major OGT isoforms: nucleocytoplasmic OGT, short OGT, and mitochondrial OGT. Nucleocytoplasmic OGT and short OGT are localized in the nucleus and cytoplasm, whereas mitochondrial OGT is present in the mitochondrial matrix. *O*-GlcNAcase, a glycosidase that removes *O*-GlcNAc from proteins, functions in a cycling fashion with OGT. OGT acts as an epigenetic "writer," whereas *O*-GlcNAcase acts as an "eraser" of this PTM by modulating biological activity of relevant nuclear proteins such as histones, RNA polymerase II, and transcription factors. The *O*-GlcNAc PTM thus plays a crucial role in nuclear homeostasis (6). The hexosamine biosynthesis pathway generates UDP-GlcNAc and UDP-GalNAc from glucose (Glc), acetyl-CoA, ATP, uridine, and amino acids (7). The UDP-hexosamine level thus depends on Glc concentration as well as salvage pathways of GalNAc and GlcNAc. *O*-GlcNAc glycan biosynthesis is affected by metabolic diseases (notably diabetes) in which Glc concentration is altered (8). *O*-GlcNAc glycosylation of nuclear proteins has a major effect on altered transcription in diabetes (9).

O-GalNAc glycans are the second most common glycan structures on secreted proteins, after *N*-glycans. Their biosynthesis is initiated by action of a multigene family of enzyme polypeptide–*N*-acetylgalactosaminyltransferases (ppGalNAc-

This work was supported by CONICET Grant PIP 11220150100226 and SeCyT, UNC Grant 05/C422 (to F. J. I.). The authors declare that they have no conflicts of interest with the contents of this article.
This work is dedicated to the memory of Mafalda C. Pellegrini-Irazoqui.
This article contains Figs. S1–S5 and Table S1.

[1] Present address: Instituto de Salud y Ambiente del Litoral, ISAL, CONICET, and Facultad de Bioquímica y Ciencias Biológicas, Universidad Nacional del Litoral, S3000ZAA Santa Fe, Argentina.
[2] To whom correspondence should be addressed. Tel./Fax: 54-351-5353855; E-mail: irazoqui@fcq.unc.edu.ar.

[3] The abbreviations used are: PTM, post-translational modification; HMC, human mononuclear cell; WGA, wheat germ agglutinin; HRP, horseradish peroxidase; OGT, GlcNAc transferase; PSM, peptide spectrum match; WB, Western blotting; ER, endoplasmic reticulum; PI, propidium iodide; DAPI, 4,6-diamidino-2-phenylindole; HPA, *H. pomatia* agglutinin; ppGalNAc-T, polypeptide–*N*-acetylgalactosaminyltransferase; VVL, *V. villosa* lectin; T2, ppGalNAc-T2; T3, ppGalNAc-T3; CBB, Coomassie Brilliant Blue; PVP, polyvinylpyrrolidone; OG, *O*-GalNAc over-glycosylated nuclei.

Ts) promoting covalent linkage of GalNAc from UDP-GalNAc donor to Ser/Thr of acceptor, yielding GalNAcα1-*O*-Ser/Thr (10). Twenty members of the ppGalNAc-T family have been found in humans. The initial step of *O*-GalNAc glycosylation is critical in defining the amino acid position of PTM on the protein and in facilitating subsequent monosaccharide incorporation. The second monosaccharide linked to GalNAcα1-*O*-Ser/Thr may be galactose (Gal) or *N*-acetylglucosamine (GlcNAc) yielding core 1 (Galβ3GalNAcα1-*O*-Ser/Thr) or core 3 (GlcNAcβ3GalNAcα1-O-Ser/Thr) glycan, respectively. The core structures are extended by action of specific glycosyltransferases to generate complex *O*-GalNAc glycans, which are synthesized mainly in Golgi (11). Truncated *O*-GalNAc glycans are commonly synthesized by epithelial tumor cells with overexpression of GalNAcα1-*O*-Ser/Thr (Tn antigen) or Galβ3GalNAcα1-*O*-Ser/Thr (T antigen) residues, possibly by deletion or loss of the glycosyltransferases elongating Tn or T antigens (12, 13), and play crucial roles in cell adhesion during the process of metastasis (14).

We examined *O*-GalNAc glycan biosynthesis in the nucleus of human cells as a PTM of nuclear proteins that may play an important role in regulating their functions. Our focus was the identification of all factors in the cell nucleus necessary for initiation of *O*-GalNAc glycan biosynthesis: the sugar donor substrate, the nuclear polypeptide GalNAc-transferase activity, an enzyme (polypeptide GalNAc-T3), and *O*-GalNAc–glycosylated proteins (the products of glycan biosynthesis).

Results

UDP-GalNAc in cell nucleus

To examine nuclear localization of several molecules, we purified HeLa cell nuclei as described previously (15). Nuclei were separated from the cytoplasm of whole cells using Nonidet P-40 detergent in appropriate buffer and by centrifugation. Purified nuclei were obtained by several washes with buffer without detergent (Fig. 1), placed in hypertonic buffer, and sonicated for disruption of nuclear membrane, and the soluble nuclear fraction (nucleoplasm) was obtained by centrifugation. Quality of purified nuclei was evaluated by confocal microscopy and Western blotting (WB) with molecular markers of cellular organelles: Golgin97 (Golgi), calreticulin (ER), tubulin (cytoplasm), and histone H3 (nucleus). Each of these methods revealed high levels of nuclear markers (PI and histone) in purified nuclei or nucleoplasm but minimal levels of cytoplasm, Golgi, and ER markers. This finding indicated that the method used for purification of nuclei was appropriate.

Biosynthesis of nucleotide sugars such as UDP-GalNAc occurs in the cytoplasm (16). UDP-GalNAc is the sugar donor substrate required for ppGalNAc-T reaction. To examine the presence of this sugar donor in the nucleus, we developed an enzymatic assay for measurement of UDP-GalNAc substrate, in which the standard curve showed an appropriate linear concentration range (Fig. S1*A*). High specificity of this enzymatic method for UDP-GalNAc was demonstrated by comparison with UDP-GlcNAc, which was found not to participate in the reaction. UDP-GalNAc level was next measured in various subcellular fractions of HeLa cells (Table 1). UDP-GalNAc concentration was very different in the nucleoplasm (0.330 μM) than in the last nuclear wash (0.015 μM), confirming the presence of this sugar nucleotide in the nucleus.

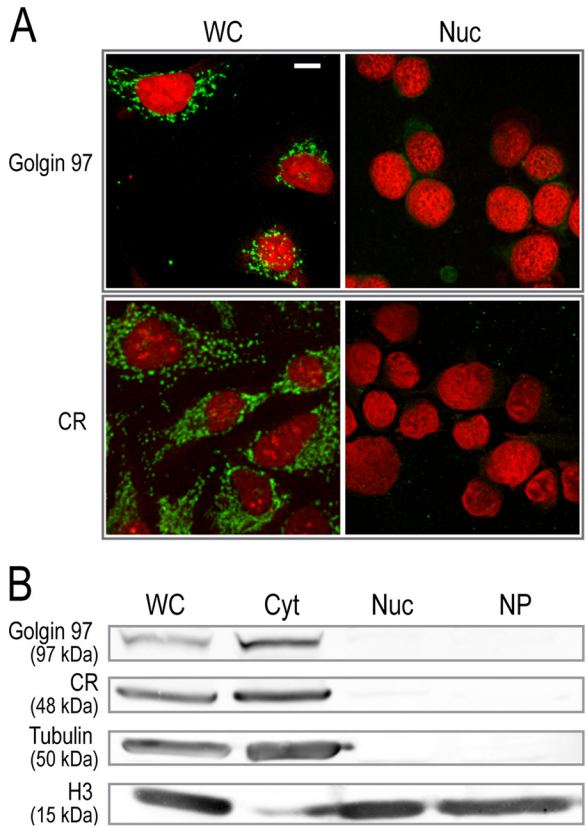

Figure 1. Purification of HeLa cell nuclei. *A,* whole cells (*WC*) and purified nuclei (*Nuc*) were analyzed by confocal fluorescence microscopy to assess nuclear purity following subcellular fractionation. Nuclei, Golgi, and ER were identified, respectively, by staining with PI (*red*), anti-Golgin 97 antibody (*green*), and anti-calreticulin (*CR*) antibody. *B,* whole cells, cytoplasm (*Cyt*), nuclei, and nucleoplasm (*NP*) samples were analyzed by WB, using anti-Golgin 97 (Golgi), anti-CR (ER), and anti-tubulin (cytosol) antibodies as cytoplasm markers, and anti-histone H3 (*H3*) antibody as nuclear marker.

To examine transport of UDP-GalNAc through the nuclear membrane, we added UDP-GalNAc to purified nuclei and measured the amount that passed inside. A substantial concentration (0.510 μM) of UDP-GalNAc was found in the nucleoplasm, reflecting the ability of this sugar nucleotide to enter the nucleus (Table 1).

ppGalNAc-T activity in the nucleus

To evaluate ppGalNAc-T activity in the nucleus, terminal glycans (products of each enzymatic reaction) were detected using various labeled lectins as probes, and specificities of biotinylated lectins were confirmed (Fig. S1, *B–D*). *Vicia villosa* lectin (VVL) and *Helix pomatia* agglutinin (HPA) recognized terminal αGalNAc residues but not βGlcNAc residues, whereas wheat germ agglutinin (WGA) primarily recognized terminal βGlcNAc residues. We assayed ppGalNAc-T activity in subcellular fractions of HeLa (human cervix), MCF7 (human breast), T47D (human mammary gland), HEK-293 (human kidney), Vero (monkey kidney) cell lines, and human mononuclear cells

Table 1
Measurement of UDP-GalNAc donor substrate in HeLa subcellular fractions

Subcellular fraction	UDP-GalNAc
	μM
Cytoplasm	24 ± 2.7
Final nuclear wash	0.015 ± 0.005
Nucleoplasm	0.330 ± 0.052
Final nuclear wash (nuclei + UDP-GalNAc)	0.060 ± 0.009
Nucleoplasm (nuclei + UDP-GalNAc)	0.510 ± 0.091

(HMC) using naked MUC1 and MUC2 as acceptor substrates and excessive UDP-GalNAc as donor substrate. The enzymatic product, αGalNAc residues, was evaluated using the VVL probe, and ppGalNAc-T activity was determined by extrapolation from the standard curve of purified MUC1αGalNAc (Fig. S1*C*). ppGalNAc-T activity was detected in the cytoplasm and nucleoplasm of analyzed cells (Table 2), whereas catalytic activity was not observed in the last nuclear wash fraction. Important ppGalNAc-T activity was detected in all analyzed nucleoplasms, reflecting the enzyme's capacity for *O*-GalNAc glycosylation of naked mucins.

ppGalNAc-T activity was next evaluated in the intact nuclei of HeLa cells. Purified nuclei were incubated with added UDP-GalNAc for 1 h at 37 °C, and the yielded glycans were detected by WB and confocal microscopy using labeled lectins. Increased numbers of terminal α-linked GalNAc residues in multiple nuclear proteins were demonstrated by WB with HPA (Fig. 2*A*). Terminal α-linkage of GalNAc to proteins was demonstrated using α-*N*-acetylgalactosaminidase (αGalNAc glycosidase). Purified nuclei previously incubated with UDP-GalNAc (OG nuclei) were washed, sonicated for nuclear membrane disruption, and incubated without or with αGalNAc glycosidase. The number of GalNAc residues in glycosylated nuclear proteins was greatly reduced in the presence of αGalNAc glycosidase, indicating that terminal GalNAc was α-anomeric. The findings that intact nuclei display GalNAc-T activity to glycosylate nuclear proteins and that this process is reversed by αGalNAc glycosidase indicate the capacity of nuclei for αGalNAc glycoprotein biosynthesis.

A comparison of the effects of UDP-GalNAc and UDP-GlcNAc preincubation on glycosylation capacity of intact nuclei is shown in Fig. 2*B*. Labeled VVL recognized an increased level of terminal *O*-GalNAc glycans when purified nuclei were added with UDP-GalNAc, whereas UDP-GlcNAc addition was not recognized by VVL. When nuclei were added with UDP-GalNAc, WB analysis with detection by WGA did not recognize an increase in *O*-glycosylation level. These findings indicate a clear distinction between initiation of *O*-GalNAc *versus* *O*-GlcNAc glycosylation of proteins in purified nuclei.

We examined *O*-GalNAc glycosylation inside the nucleus by confocal microscopy of purified intact nuclei of HeLa cells. Constitutive *O*-GalNAc residues in these nuclei are shown using VVL (Fig. 3*A*), as well as HPA and anti-Tn antibody (Fig. S2) (*top*). The interaction of VVL with constitutive *O*-GalNAc residues of intact nuclei was inhibited in the presence of GalNAc (Fig. S3). Incubation of nuclei with added UDP-GalNAc enhanced the product of *O*-GalNAc glycosylation (Fig. 3*A* and Fig. S2, *bottom*). Z-stacks of purified nuclei showed that in

Table 2
Measurement of ppGalNAc-T activity in subcellular fractions of different cells using MUC1 and MUC2 peptides as acceptor substrate

	ppGalNAc-T activity (mean ± S.D. error)											
	Total[a] (microunits)					Specific (microunits/mg)						
	HeLa	MCF-7	T47D	HEK-293	Vero	HMC	HeLa	MCF-7	T47D	HEK-293	Vero	HMC
A. $MUC2_{33}$ acceptor												
Cytoplasm	90.0 ± 6.7	74 ± 14	71.1 ± 3.2	58 ± 21	72 ± 19	55 ± 12	21.3 ± 1.6	14.7 ± 2.7	16.5 ± 1.8	26.7 ± 9.8	20.5 ± 5.3	4.6 ± 1.0
Final nuclear wash	ND[b]	ND	ND	ND	ND	ND	ND	ND	ND	ND	ND	ND
Nucleoplasm	48.1 ± 5.9	22.5 ± 3.4	17.6 ± 2.3	30.2 ± 3.4	20.5 ± 4.4	10.5 ± 1.3	24.2 ± 2.9	25.2 ± 3.8	30.2 ± 3.9	26.5 ± 3.0	27.8 ± 6.0	10.1 ± 1.3
B. $MUC1_{24}$ acceptor												
Cytoplasm	35.4 ± 3.1	40.2 ± 2.0	10.5 ± 1.2	39,4 ± 2.4	34.1 ± 1.3	4.80 ± 0.96	5.60 ± 0.49	5.90 ± 0.30	2.44 ± 0.28	5.86 ± 0.36	4.86 ± 0.18	ND
Final nuclear wash	ND	ND	ND	ND	ND	ND	ND	ND	ND	ND	ND	
Nucleoplasm	17.59 ± 0.57	10.15 ± 0.66	5.78 ± 0.70	15,17 ± 0.67	17.2 ± 1.6	ND	9.86 ± 0.32	5.83 ± 0.38	2.38 ± 0.30	9.03 ± 0.40	11.1 ± 1.0	ND

[a] Total ppGalNAc-T activity present in cytoplasm/final nuclear wash/nucleoplasm from 10^7 cells.
[b] ND means not detected; <1.00 ± 0.20.

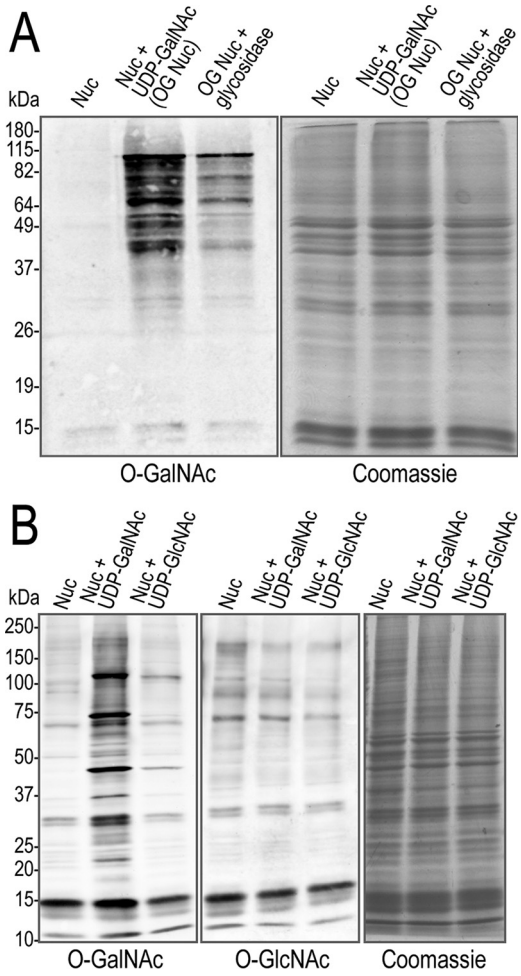

Figure 2. α-Linked GalNAc glycosylation of nuclear proteins in HeLa cells. *A,* purified nuclei (*Nuc*), over-glycosylated nuclei obtained by preincubation of purified nuclei with 250 μM UDP-GalNAc (*OG Nuc*), and OG nuclei treated with αGalNAc glycosidase (*OG Nuc + glycosidase*) were analyzed by SDS-PAGE (15% acrylamide) using biotin–HPA for *O*-GalNAc residue detection on proteins by WB. OG nuclei incubated without αGalNAc glycosidase showed identical *O*-GalNAc profile to UDP-GalNAc line (data not shown). Loading controls (*right*): identical running gels stained with CBB. *B,* purified nuclei (*Nuc*), over-glycosylated nuclei obtained by incubation of purified nuclei with 250 μM UDP-GalNAc (*Nuc + UDP-GalNAc*), and purified nuclei incubated with 250 μM UDP-GlcNAc (*Nuc + UDP-GlcNAc*) were analyzed by SDS-PAGE (4–20% acrylamide gradient) and detected with biotin–VVL for *O*-GalNAc glycan detection (*left*) or with biotin–WGA for *O*-GlcNAc glycan detection by WB (*middle*). Loading controls as in *A*.

both situations (constitutive glycosylation and GalNAc over-glycosylation), *O*-GalNAc residues were present in the nucleus, indicating the occurrence of *O*-GalNAc glycosylation within the nucleus. We next used fluorescence confocal imaging to quantify levels of *O*-GalNAc residues following *O*-GalNAc over-glycosylation of purified nuclei. Representative images of measured nuclei and OG nuclei, stained with VVL and PI, are shown in Fig. 3*B*. Levels of terminal αGalNAc residues per nucleus were evaluated. Over-glycosylated *O*-GalNAc resulted in a 4.7-fold (638.9/135.4) increase of *O*-GalNAc residues in purified nuclei (Fig. 3*C*), indicating that nuclear GalNAc-T activity produced a significant increase of *O*-GalNAc glycosylation.

Finally, we studied ppGalNAc-T nuclear activity in intact CHO ldlD cells. This cell line lacks a functional UDP-Gal-4-epimerase and therefore relies on GalNAc salvaged from the medium for the synthesis of UDP-GalNAc. CHO ldlD cells were grown in media supplemented without (−GalNAc) or with (+GalNAc) GalNAc, and the yielded glycans were detected by confocal microscopy using labeled lectins (Fig. 4). Incubation of cells with GalNAc in growing media enhanced the product of *O*-GalNAc glycosylation (Fig. 4*A*), resulting in a 5.8-fold increase in nuclear signal in +GalNAc CHO ldlD cells (Fig. 4*B*). The subcellular distribution of terminal GalNAc in the cells reveals that a high portion of the signal coincides with the nuclear marker DAPI (Fig. 4*C*), indicating nuclear ppGalNAc-T activity in intact cells.

Nuclear localization of ppGalNAc-T3

GalNAc-Ts are localized mainly in the Golgi; however, a few ppGalNAc-T isoforms have been reported in other locations, *e.g.* ER (17). We examined subcellular localization of isoforms ppGalNAc-T2 (T2) and ppGalNAc-T3 (T3), with emphasis on T3. Fluorescence microscopy assays with anti-human T2 and T3 antibodies was performed to study subcellular localization of these isoforms in HeLa, MCF-7, T47D, SK-N-AS, HEK-293, MRC-5, Vero, and HMC cells (Fig. S4). T2 showed a characteristic Golgi staining pattern in these cells (Fig. S4*A*). T3 showed a nuclear staining pattern (overlap with nuclear marker DAPI) in HeLa, MCF7, SK-N-AS, HEK-293, MRC-5, Vero, and HMC, but not T47D. Distribution of T3 coincided mainly with the nuclei, whereas T2 showed a Golgi distribution. Evidence for the specificity of anti-T3 antibody was provided by WB and competitive immunofluorescence assay using purified soluble T3. Recombinant human soluble T3 was expressed in insect cells and purified by affinity chromatography. We demonstrated the purity of T3 by SDS-PAGE with Coomassie Brilliant Blue (CBB) staining, which revealed a protein of appropriate molecular mass (72 kDa) (Fig. S4*B*). Anti-T3 antibody, on WB, recognized a protein with corresponding molecular weight. This antibody also recognized a unique protein with molecular weight corresponding to that of T3 in HeLa cell homogenate. In competitive immunofluorescence assay, recognition of T3 by the antibody in HeLa cells was inhibited by the presence of purified soluble T3 (Fig. S4*C*). The presence of soluble T3 strongly reduced both the dot-shaped nuclear pattern and the Golgi staining pattern of T3, indicating the ability of antibody to specifically recognize endogenous T3 in HeLa cells.

T3 nuclear distribution was analyzed by confocal microscopy in purified nuclei, compared with whole HeLa cells (Fig. 5). Delimitation of the nucleus was detected by staining of nucleic acids with PI, and T3 was detected with anti-T3 antibody. Purification of nuclei removed T3 localized in Golgi but conserved nuclear T3, as observed in many purified nuclei (Fig. 5*A*). Co-localization of T3 with PI was observed in zoomed regions of whole-cell nuclei and purified nuclei. Orthogonal views (*x, y* and *x, z* views) of nuclear Z-stacks reveal co-localization of T3 with PI through the Z planes (Fig. 5*B*), confirming localization of T3 inside the nucleus of HeLa cells.

Identification of O-GalNAc–glycosylated nuclear proteins

Proteins with *O*-GalNAc glycans were identified using a combination of affinity chromatography of immobilized VVL to select *O*-GalNAc glycoproteins and MS for protein identifi-

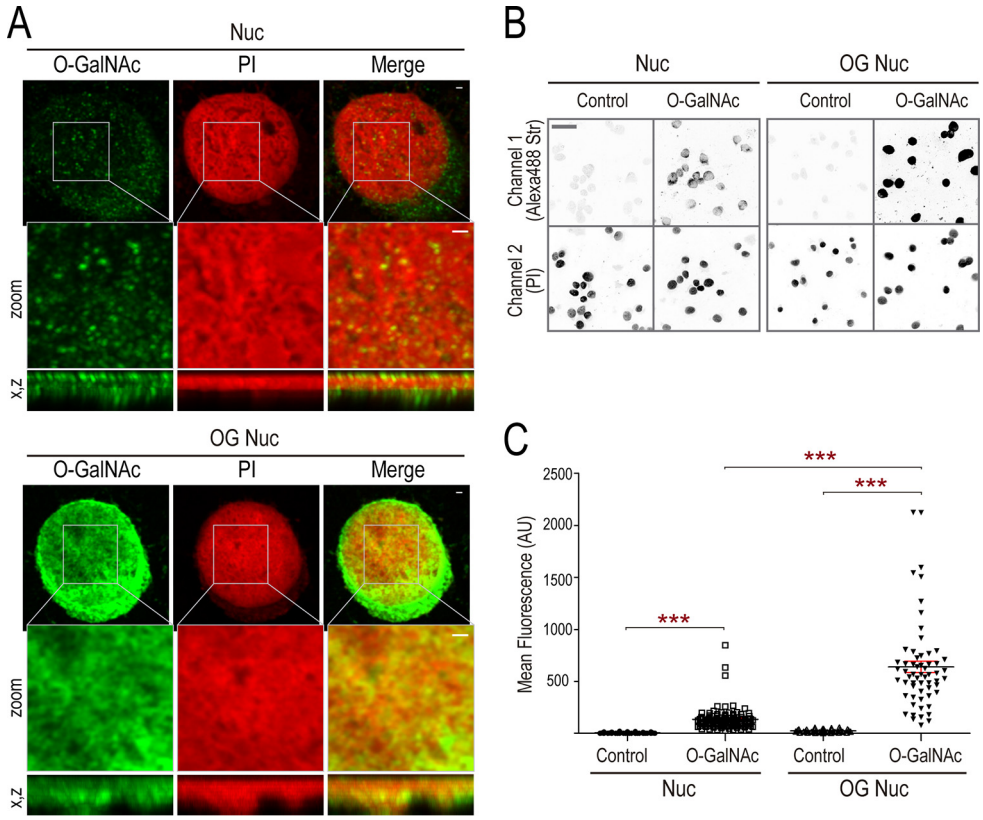

Figure 3. Biosynthesis of *O*-GalNAc glycans in HeLa cell nucleus. *A,* representative images from confocal fluorescence microscopy of purified nuclei (*Nuc, top*) and OG nuclei incubated with UDP-GalNAc (*OG Nuc, bottom*). *O*-GalNAc residues on proteins were detected with Alexa 488–streptavidin/biotin–VVL (*green*), and nuclei were stained with PI (*red*). Images of the nuclear plane are shown as individual channels and *merge* mode. *Square,* zoomed nuclear region, also shown in *x, y* and *x, z* orthogonal views, show detailed distribution of *O*-GalNAc glycans in the nucleus. *Scale bar,* 1 μm. *B,* representative confocal images (inverted *gray* pseudocolored) showing *O*-GalNAc glycosylation level (detected with Alexa 488–streptavidin/biotin–VVL) (*top*) in purified nuclei (*Nuc*) and purified OG nuclei (*OG Nuc*). *Controls:* Alexa 488–streptavidin without biotin–VVL. Nuclei were stained with PI (*bottom*). *Scale bar,* 1 μm. *C,* quantitative analysis of *O*-GalNAc glycosylation level under conditions as in *B*. Fluorescence of channel 1 (Alexa 488) (*AU*, arbitrary units) per nucleus was measured in 60 nuclei. *Lines,* mean arbitrary units. Means compared by unpaired *t* test indicate significant difference; *** ($p < 0.001$). See also Fig. S2.

cation. Nucleoplasm from purified nuclei (constitutive *O*-GalNAc glycosylated nuclear proteins) and nucleoplasm from OG nuclei of HeLa cells were analyzed. Each nucleoplasm was divided into two equal parts: one part was loaded onto streptavidin–agarose column (−VVL column) to identify unspecific adsorption, and the other part was loaded onto VVL-biotin/streptavidin–agarose column (+VVL column) to retain *O*-GalNAc–glycosylated proteins. Differences of retained proteins between the +VVL and −VVL column were evaluated by SDS-PAGE with colloidal CBB staining (Fig. S5). Proteins from gel bands were digested, and peptides were identified by MS. The criterion for the presence of *O*-GalNAc glycans on proteins was the identification of ≥2 high-quality peptides per protein, and peptide spectrum matches (PSM) ratio ≥3 (see "Experimental procedures"). Identified *O*-GalNAc–glycosylated proteins in order of decreasing PSM ratio, their subcellular localization, and main protein function according to UniProt (http://www.uniprot.org),[4] are listed in Table 3. Two proteins were identified as endogenously *O*-GalNAc–glycosylated in the nucleoplasm: 40S ribosomal protein S6 (RPS6) and S3 (RPS3) (Table 3A). They are both localized in nuclei, according to UniProt. Twenty five glycoproteins were detected in OG nucleoplasm, indicating the predominance of nuclear localization in this group (Table 3B). PSM ratios of RPS6 and RPS3 were 4 and 3, respectively; in contrast, some proteins in the OG nucleoplasm group had much higher PSM ratios (30 in the case of prelamin-A/C). These findings suggest a direct correlation between *O*-GalNAc over-glycosylation, major glycoprotein retention by +VVL column, and increased PSM ratio of proteins in the nucleoplasm. Incubation of purified intact nuclei with UDP-GalNAc led to detection of OG proteins localized predominantly in the nucleus, indicating that *O*-GalNAc glycosylation occurs inside the nucleus. The identified nuclear proteins with the highest *O*-GalNAc glycosylation levels were prelamin-A/C (PSM ratio = 30) and lamin B1 (LMNB1) (PSM ratio = 22). We therefore examined nuclear *O*-GalNAc glycosylation of lamins in more detail.

O-GalNAc glycosylation of LMNB1

Software programs are available with accepted algorithms that allow theoretical predictions regarding *O*-GalNAc glycosylation sites on proteins. Prediction of *O*-GalNAc glycosylation on LMNB1 was made using the NetOGlyc 4.0 Server (www.cbs.dtu.dk/services/NetOGlyc/)[4] (18). LMNB1 had a large number of sites with a high likelihood of *O*-GalNAc glycosylation (Table S1), consistent with our identification of

[4] Please note that the JBC is not responsible for the long-term archiving and maintenance of this site or any other third party hosted site.

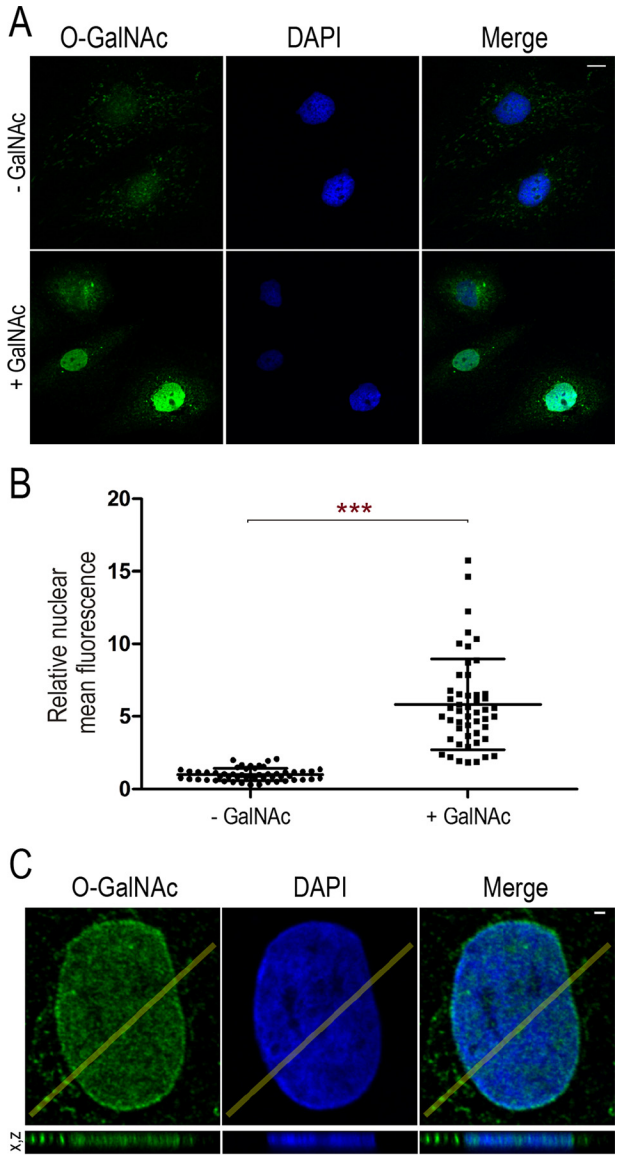

Figure 4. Nuclear *O*-GalNAc glycosylation in CHO ldlD cells. *A,* representative images from confocal fluorescence microscopy of CHO ldlD cells grown in media without GalNAc (−GalNAc; *top*) or supplemented with GalNAc (+GalNAc; *bottom*). *O*-GalNAc residues on proteins were detected with Alexa 488–streptavidin/biotin–VVL (*green*) and nuclei stained with DAPI (*blue*). Images are shown as individual channels and *merge* mode. *Scale bar,* 10 μm. *B,* quantitative analysis of nuclear *O*-GalNAc glycosylation level under conditions as in *A*. Mean fluorescence in nuclear region per cell was measured in −GalNAc or +GalNAc growing conditions. Values are expressed as relative to the lower average fluorescence value. *Lines,* mean ± S.D. ($n = 56–60$ cells). Means compared by unpaired *t* test indicate significant difference; *** ($p < 0.001$). *C,* confocal Z-stack images of a representative CHO ldlD cell grown in media with GalNAc. Axial views (*x, z*) (*bottom panel*) along the *yellow line* displayed in the *upper panel* allows us to appreciate the distribution of *O*-GalNAc terminals (*green*) outside and inside of the nucleus (*blue*). Images are shown as individual channels and *merge* mode. *Scale bar,* 1 μm.

LMNB1 as a highly *O*-GalNAc– glycosylated protein following incubation of purified nuclei with UDP-GalNAc.

O-GalNAc glycosylation of LMNB1 was evaluated by co-localization and FRET assays using fluorescence confocal microscopy. Labeled Cherry–LMNB1 was overexpressed in HeLa cells. Purified nuclei from these cells were incubated without or with UDP-GalNAc, and the resulting *O*-GalNAc glycosylation was studied using biotin–VVL and Alexa 488–streptavidin.

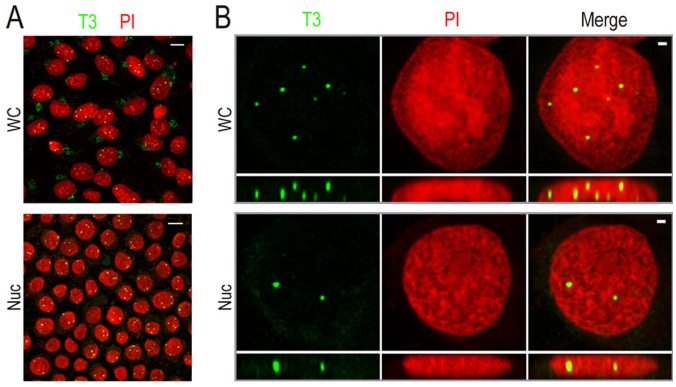

Figure 5. Localization of ppGalNAc-T3 (*T3*) in the nucleus of HeLa cells. *A,* representative images from confocal fluorescence microscopy of whole cells (*WC*; *top*) and purified nuclei (*Nuc*; *bottom*) showing T3 stained with anti-T3 antibody (*green*) and nuclei stained with PI (*red*). *Scale bar,* 10 μm. *B,* maximum intensity projection and corresponding axial views (*x, z*) of confocal Z-stack images of whole cells and purified nucleus with notations as in *A*. Images are shown as individual channels and merge mode. *Scale bar,* 1 μm.

Correlation analysis between VVL (channel 1) and LMNB1 (channel 2) was performed for control nuclei and OG nuclei (Fig. 6*A*). Correlation of signals was stronger in the OG nuclei, as a consequence of nuclear GalNAc-T activity. Fluorescence profiles of the two channels were analyzed and showed greater accompaniment of fluorescent intensities in the OG nuclei. Comparison of fluorograms showed enhanced correlation between LMNB1 and *O*-GalNAc residues following incubation with UDP-GalNAc. The correlation was quantified by Pearson's correlation coefficient for nuclei without or with UDP-GalNAc preincubation and glycosylation detected with biotin–VVL (αGalNAc) or biotin–WGA (βGlcNAc) (Fig. 6, *B* and *C*). The correlation coefficient between LMNB1 and *O*-GalNAc residues showed a 4.1-fold (0.630/0.151) increase after UDP-GalNAc incubation and biotin–VVL detection, but no significant change after biotin–WGA detection. These findings suggest that LMNB1 is *O*-GalNAc– glycosylated in the nucleus.

O-GalNAc glycosylation of LMNB1 was further evaluated by acceptor photobleaching/FRET. Again, purified nuclei from Cherry–LMNB1-overexpressing cells were incubated without or with UDP-GalNAc to study LMNB1 *O*-GalNAc glycosylation, and biotin–VVL or biotin–WGA with Alexa 488–streptavidin were used for *O*-glycan detection. FRET index for each experimental condition was calculated as described under "Experimental procedures." A map of FRET index was prepared, corresponding to representative images of nuclei preincubated without or with UDP-GalNAc and detected with biotin–VVL (Fig. 7*A*) or biotin–WGA (Fig. 7*B*). FRET index was significantly higher for OG nuclei with *O*-GalNAc termini of LMNB1 detected with biotin–VVL (Fig. 7*C*). Detection with biotin–WGA gave no notable difference for control nuclei *versus* OG nuclei (Fig. 7, *B* and *D*). The increase in FRET index with biotin–VVL detection confirms that *O*-GalNAc residues are added to LMNB1 in the nucleus, showing the ability of nuclei to synthesize *O*-GalNAc glycans.

Discussion

PTMs are essential modulators of cell homeostasis, play key roles in protein function and localization, and regulate cell

Table 3
Identification of *O*-GalNAc glycosylated proteins from HeLa cell nucleoplasm
RNP is ribonucleoprotein.

PSM ratio	Accession no.	Name	Subcellular localization	Function
A. *O*-GalNAc glycosylated				
4	P62753	40S ribosomal protein S6 (RPS6)	Nucleus, nucleolus, cytoplasm	RNA binding, translational initiation
3	P23396	40S ribosomal protein S3 (RPS3)	Nucleus, nucleolus, cytoplasm	DNA repair, translation
B. Overglycosylated *O*-GalNAc				
30	P02545	Prelamin-A/C (LMNA)	Nuclear envelope, nucleoplasm, speckle	Nuclear assembly, chromatin organization
22	P20700	Lamin-B1 (LMNB1)	Nuclear envelope, nucleoplasm	Framework for nuclear envelope, interacts with chromatin
17	P23246-2	Isoform short of SFPQ (SFPQ)	Nuclear matrix, paraspeckles, cytoplasm	Splicing factor, regulation of transcription
8	Q15233	Non-POU domain–containing octamer-binding protein (NONO)	Nucleolus, paraspeckles, nucleoplasm	RNA processing, regulation of transcription
8	P36957	Dihydrolipopolylysine residue succinyltransferase (OGDC-E2)	Nucleus, mitochondria	Amino acid degradation
7	Q03252	Lamin-B2 (LMNB2)	Nuclear envelope, nuclear inner membrane	Framework for nuclear envelope, interacts with chromatin
6	P04843	Dolichyl-diphospho-oligosaccharide–protein glycosyltransferase S1 (RPN-I)	ER	Protein glycosylation, RNA binding
5	P23396	40S ribosomal protein S3 (RPS3)	Nucleus, nucleolus, cytoplasm	DNA repair, translation
4.7	P38159	RNA-binding motif protein, X chromosome (RBMX)	Nucleus, RNP complex	RNA processing, gene expression
4	Q08211	ATP-dependent RNA helicase A (DHX9)	Nucleolus, RNP complex, cytoplasm	Transcriptional activator, RNA processing
4	P61979-3	Heterogeneous nuclear RNP K isoform 3 (hnRNP K)	Nucleoplasm, spliceosome, cytoplasm	Transcription activation and repression, RNA processing
4	P49458	Signal recognition particle 9-kDa protein (SRP9)	RNP complex, cytoplasm	Negative regulation of translation
3.5	P62269	40S ribosomal protein S18 (RPS18)	Nucleus, nucleoplasm, cytoplasm	Nuclear-transcribed mRNA catabolic process, translational initiation
3.5	P61247	40S ribosomal protein S3a (RPS3A)	Nucleus, nucleolus, cytoplasm	nuclear-transcribed mRNA catabolic process, translational initiation
3	P62263	40S ribosomal protein S14 (RPS14)	Nucleolus, nucleoplasm, cytosol	Regulation of transcription, translation
3	P08865	40S ribosomal protein SA	Nucleus, nucleoplasm, cytoplasm	rRNA export and processing, translation
3	P05388	60S acidic ribosomal protein P0 (RPLP0)	Nucleus, cytoplasm	rRNA processing, translation
3	P05387	60S acidic ribosomal protein P2 (RPLP2)	RNP complex, cytosol	rRNA processing, elongation
3	P68104	Elongation factor 1-α1 (EF-1-α-1)	Nucleolus, cytoplasm	Elongation factor, transcription regulation
3	P35232	Prohibitin (PHB)	Nucleus, cytoplasm, mitochondria	Inhibits DNA synthesis, cellular proliferation
3	Q99623	Prohibitin-2 (PHB2)	Nucleus, cytoplasm, mitochondria	Transcriptional repressor
3	Q9Y262	Eukaryotic translation initiation factor 3 subunit L (eIF3l)	Nucleoplasm, nucleolus, cytoplasm	Translation initiation factor activity
3	P21333–2	Filamin-A isoform 2 (FLNA)	Nucleus, nucleolus, cytoplasm	Promotes orthogonal branching of actin filaments
3	O75533	Splicing factor 3B subunit 1 (SF3B1)	Speckles, nucleoplasm	RNA splicing, gene expression
3	Q15149	Plectin (PLEC)	Cytoplasm	Interlinks intermediate filaments, RNA binding

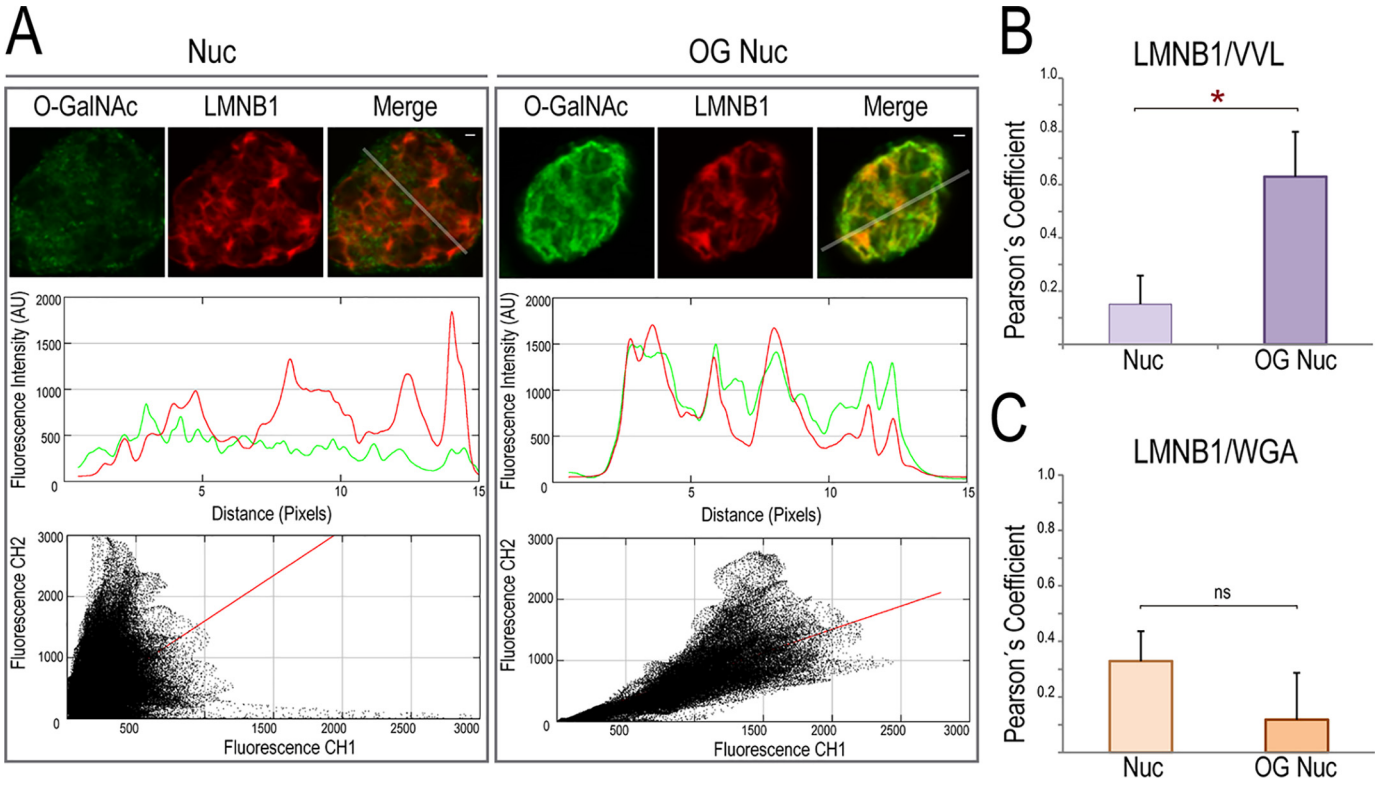

Figure 6. Correlation study of LMNB1 and *O*-GalNAc glycosylation in HeLa cells. *A,* purified nuclei (*Nuc*) preincubated without or with UDP-GalNAc (*OG Nuc*) of cells expressing Cherry–LMNB1 (*red*) were fixed and stained with VVL for detection of *O*-GalNAc residues (*green*) and correlation analysis of *O*-GalNAc glycosylation (*1st channel*) and LMNB1 (*2nd channel*). *Top panels,* representative confocal fluorescence images of nuclei and OG nuclei as separated channels and *merge* mode. *Yellow color,* overlap of signals. *Scale bar,* 10 μm. *Middle panel,* fluorescence profiles of the two channels along the *white line* shown in the *merge* images. Stronger correlation is seen for OG nuclei between *O*-GalNAc glycosylation (*green line*) and LMNB1 (*red line*). *Bottom panel,* corresponding fluorograms between *1st* and *2nd channels* for nuclei and OG nuclei. *B,* quantification of Pearson's correlation coefficient between *O*-GalNAc glycosylation (detected with VVL) and Cherry–LMNB1 in nuclei and OG nuclei. *C,* quantification of Pearson's correlation coefficient between WGA (which detects *O*-GlcNAc termini; control) and LMNB1 in nuclei and OG nuclei. Data shown are mean Pearson's correlation coefficient ± S.E. ($n = 5$). Means compared by Mann-Whitney test indicate significant difference; * ($p < 0.05$) or *ns* (not significant).

interactions in a variety of biological processes. Many nuclear proteins undergo PTMs (notably acetylation, methylation, phosphorylation, ubiquitination, and glycosylation in mammalian cells) that affect gene expression and nuclear physiology (7, 19, 20). We studied biosynthesis of *O*-GalNAc glycans in the nucleus of human cells and documented the presence of all factors necessary for initiation of *O*-GalNAc protein glycosylation: the sugar donor substrate, catalytic ppGalNAc-T activity, an enzyme (polypeptide GalNAc-T3), and products of the enzymatic reaction.

O-GalNAc glycosylation of proteins is initiated by ppGalNAc-Ts catalyzing covalent linkage of GalNAc to the hydroxyl residue of Ser or Thr. This enzymatic reaction requires two substrates: a sugar donor (UDP-GalNAc) and a protein acceptor substrate. Mucin-type domains are more frequently *O*-GalNAc– glycosylated in amino acid sequences having predominant presence of Ser and Thr, surrounding Pro. Proteins with mucin-type domains are widely distributed in cells, including the nucleus. We developed a highly specific and sensitive quantification method to detect UDP-GalNAc substrate in nuclei, and we used it to measure a 0.330 μM concentration of UDP-GalNAc in HeLa cell nucleoplasm. Hart and Akimoto (21) reported a similar concentration (0.50 μM) of UDP-GlcNAc in the nucleoplasm, whereas Bond and Hanover (22) described UDP-GlcNAc concentrations ranging from 2 to 30 μM in the cytoplasm, nuclei, and mitochondria. As in glycosylation reactions, two substrates are required, and the relevance of this UDP-GalNAc concentration in the nucleus is conditioned by enzyme's K_m value of donor substrate, which is depending on the nuclear amino acid sequence of the acceptor substrate. When we incubated purified intact nuclei with added UDP-GalNAc, we observed a substantial concentration (0.510 μM) of UDP-GalNAc in the nucleoplasm. These findings reflect the ability of UDP-GalNAc to reach the nucleoplasm by crossing the nuclear membrane. UDP-GalNAc synthesized in cytoplasm is thus able to cross the nuclear membrane and be available as a sugar donor substrate for nuclear ppGalNAc-Ts. Bond and Hanover (22) described similar nuclear membrane permeability and the ability of UDP-GlcNAc to enter the nucleus. Concentrations of UDP-GalNAc and its epimer UDP-GlcNAc are directly affected by nutrient availability. Similarly to previous findings for UDP-GlcNAc concentration, metabolic alterations that affect the UDP-GalNAc concentration may alter nuclear ppGalNAc-T activity and thereby regulate levels of *O*-GalNAc glycosylation on nuclear proteins.

We demonstrated significant ppGalNAc-T activity in all nucleoplasms of several cells, reflected by the catalytic capacity to link GalNAc to naked MUC1 and MUC2 (Table 2). HMC nucleoplasm showed ppGalNAc-T activity with MUC2 accep-

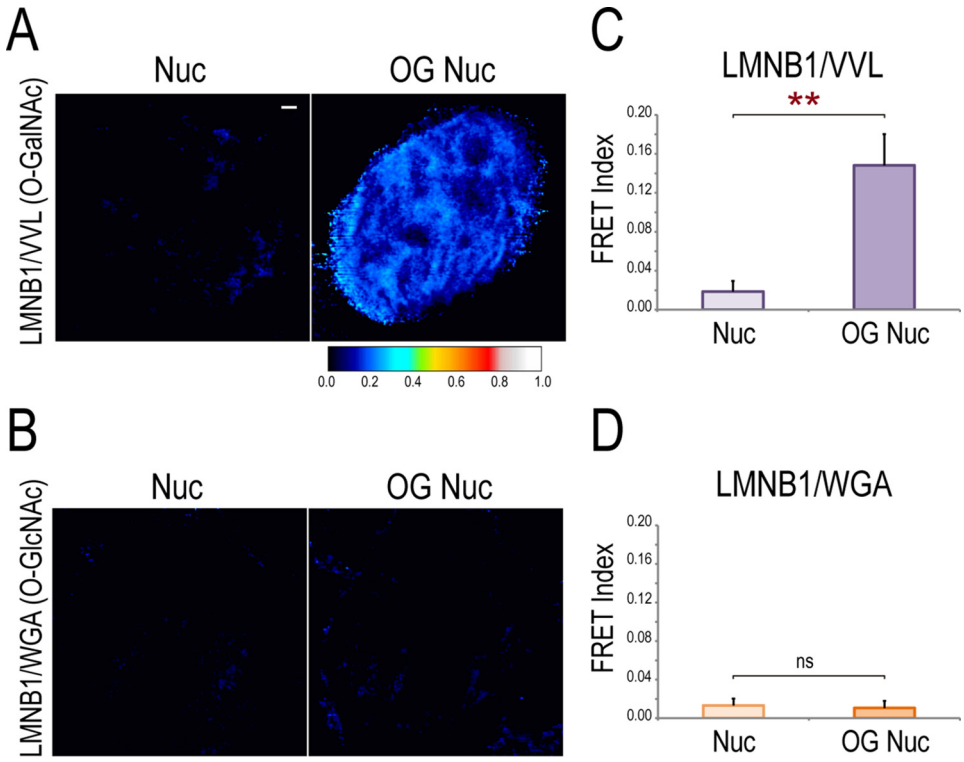

Figure 7. *O*-GalNAc glycosylation of lamin-B1 (LMNB1) in nuclei of HeLa cells. *A* and *B,* nuclear *O*-GalNAc glycosylation of LMNB1 was analyzed by acceptor photobleaching FRET in purified nuclei expressing Cherry–LMNB1, preincubated without (*Nuc*) or with UDP-GalNAc (*OG Nuc*). *O*-Glycosylation was detected with Alexa 488–streptavidin/biotin–VVL (αGalNAc residues) or Alexa 488–streptavidin/biotin–WGA (βGlcNAc residues, control). *A,* representative images of VVL (*O*-GalNAc glycosylation) and LMNB1 (*top*) or WGA (*control*) and LMNB1 (*bottom*) FRET index map in purified nuclei and OG nuclei. *Color-code bar* indicates FRET index (0 to 1) for each pixel. For OG nuclei, FRET is between VVL and LMNB1, indicating that LMNB1 is *O*-GalNAc–glycosylated in the nucleus. *Scale bar,* 1 μm. *C* and *D,* statistical analysis of FRET index of LMNB1 and VVL (*O*-GalNAc terminals) (*C*), and LMNB1 and WGA (*D*), in purified nuclei preincubated without (*Nuc*) or with UDP-GalNAc (*OG Nuc*). Data shown are mean FRET index ± S.E. ($n = 5$). Means compared by Mann-Whitney test indicate significant difference; ** ($p < 0.01$) or *ns* (not significant).

tor, but it was not observed on the MUC1 acceptor. It could be explained because this enzyme activity is conditioned by the ppGalNAc-T isoforms present in the nucleoplasm of each cellular type. The fact that ppGalNAc-T activity is present in nontumoral (HEK-293, Vero, and HMC) and tumoral (HeLa, T47D, and MCF-7) nucleoplasms, as well as in nuclei of CHO ldlD cells suggests that the presence of *O*-GalNAc glycosylation machinery in the nucleus would be a normal physiological process. ppGalNAc-T activity was also observed in HeLa purified nuclei, and incubation of purified nuclei with added donor substrate (UDP-GalNAc) enhanced the *O*-GalNAc glycosylation of several proteins. Studies of α-anomeric GalNAc linkage to nuclear proteins, and linkages of various controls (including UDP-GlcNAc and WGA), showed that the *N*-acetylhexosamine linkage in this case is not βGlcNAc, as described previously for other nuclear proteins. Following preincubation of purified nuclei with UDP-GalNAc, confocal microscopy assays revealed *O*-GalNAc glycosylation inside the nucleus. Another key point in this study was the demonstration of nuclear ppGalNAc-T activity in intact cells. CHO ldlD cells are a robust model for studying the initiation of *O*-GalNAc glycosylation given that they are deficient in UDP-Gal and UDP-GalNAc 4-epimerase and are therefore unable to synthesize UDP-Gal or UDP-GalNAc. The addition of GalNAc to CHO ldlD cell culture medium allowed us to demonstrate that the incorporation of *O*-GalNAc terminals is also occurring in the nuclei of intact cells.

Localization in nuclei of ppGalNAc-T3 (T3), an enzyme that initiates *O*-GalNAc glycan biosynthesis, was observed by microscopy in different whole cells and purified nuclei. Glycosyltransferases are generally localized in Golgi of mammalian cells (11), but other subcellular localizations have been reported, *e.g.* sialyltransferase in plasma membrane (23), *O*-GlcNAc-transferase in mitochondria, cytoplasm, and nuclei (24), and ppGalNAc-Ts in ER (17). We demonstrate here the nuclear localization of T3 in different cells, similarly reported by Human Protein Atlas in human RT4 cell nuclei (https://www.proteinatlas.org/ENSG00000115339-GALNT3/cell#img (26)).[4] The ppGalNAc-T activity observed in T47D nucleoplasm, without T3 nuclear localization, is consistent with the presence of additional ppGalNAc-T isoforms in the nucleus. The Human Protein Atlas (www.proteinatlas.org (26))[4] reports the presence of six isoforms of the ppGalNAc-T family (ppGalNAc-T5, -T6, -T7, -T10, -T14, and -T16) in the nuclei of various human cell lines (25, 26).

Identification of *O*-GalNAc–glycosylated nuclear proteins indicated the occurrence of a PTM not previously described in the nuclei and suggested that *O*-GalNAc glycosylation may modulate functions of certain nuclear proteins. Accordingly, we studied constitutive and over-glycosylated *O*-GalNAc nuclear proteins. *O*-GalNAc–glycosylated proteins from HeLa nucleoplasm were purified on an affinity chromatography column using immobilized VVL, and retained glycoproteins were identified by MS. Two proteins (RPS6 and RPS3), both known

to be localized in nucleus and cytoplasm, were identified as constitutively *O*-GalNAc– glycosylated. It is likely that numerous other nuclear proteins are constitutively *O*-GalNAc–glycosylated but were not retained on the VVL column because this lectin recognizes glycoproteins with terminal GalNAc residues. Constitutive *O*-GalNAc glycosylation could thus continue the glycan biosynthetic pathway with capping of the initial αGalNAc residue and evade VVL recognition.

Incubation of purified nuclei with UDP-GalNAc allowed identification of numerous *O*-GalNAc– glycosylated proteins. Of 25 such proteins (Table 3*B*), 22 are localized in the nucleus. This finding confirms that biosynthesis of *O*-GalNAc glycans occurs in the nucleus, because the approach involves incubation of purified nuclei with UDP-GalNAc. Among the 22 proteins as above, PSM ratios were highest for pre-LMNA/C and LMNB1. These two proteins, and LMNB2, are essential components of the nuclear lamina, a filamentous layer located between the inner nuclear membrane and peripheral heterochromatin that plays crucial roles in nuclear organization and interactions with the genome, including promoter regions that modulate gene expression (27, 28). Other nuclear proteins identified as *O*-GalNAc– glycosylated (Table 3*B*) include the following: (i) splicing factor, proline- and glutamine-rich (SFPQ) and non-POU domain-containing octamer-binding protein (NONO), characteristic components of nuclear body paraspeckles, which are involved in control of gene expression during cellular processes such as differentiation, viral infection, and stress responses (29); (ii) ribosomal proteins that are involved in translation, DNA repair (RPS3), and mRNA catabolism (RPS18 and RPS3A) (30–32); (iii) RNA-binding motif protein, X chromosome, and ATP-dependent RNA helicase A (DHX9) involved in gene expression, transcriptional activation, and RNA processing (33, 34). In view of the varied functions of identified proteins as above, nuclear *O*-GalNAc glycosylation may play essential roles in nuclear homeostasis.

Additional methods were applied for the study of LMNB1, which had a high PSM ratio, and a prediction of highly probable *O*-GalNAc glycosylation. Co-localization analysis of *O*-GalNAc residues and LMNB1 revealed an increase of Pearson's correlation coefficient as a consequence of *O*-GalNAc over-glycosylation. Similarly, FRET index between *O*-GalNAc glycans and LMNB1 was increased by *O*-GalNAc over-glycosylation. Co-localization and FRET studies thus confirmed the nuclear *O*-GalNAc glycosylation of LMNB1, in agreement with findings from affinity chromatography and MS. Nuclear lamins play key roles in nuclear organization, nuclear physiology, and gene expression (35, 36). They undergo extensive PTMs (*e.g.* phosphorylation and sumoylation) that help determine their localization and dynamics (37, 38). Lamins can also be ADP-ribosylated or *N*-glycosylated (7, 39). Wang *et al.* (40) reported that LMNA was *O*-GlcNAc– glycosylated in HeLa cells. By using other experimental approaches (SimpleCell strategy), Steentoft *et al.* (18) reported the presence of *O*-GalNAc– glycosylated nuclear proteins, and Yang *et al.* (41) has described *O*-GalNAc glycosylation sites of Lamin-A/C, 40S ribosomal protein SA, and elongation factor 1-α1 (EF-1-α-1) nuclear proteins of CHO cells, in agreement with our results. No previous study has presented experimental evidence of LMNB1 *O*-glycosylation. LMNB1 plays crucial roles in high-order chromatin organization, DNA replication, and transcriptional activity (42, 43).

In conclusion, this study provides solid evidence of *O*-GalNAc glycan biosynthesis machinery in the nucleus of human cells. All factors necessary for initiation of such biosynthesis are present in the nucleus: the required donor substrate (UDP-GalNAc); nuclear ppGalNAc-T activity; an enzyme (T3); and the identified *O*-GalNAc– glycosylated proteins in the nucleus. This is the first demonstration of *O*-GalNAc glycosylation of nuclear human proteins. Because UDP-GalNAc biosynthesis is sensitive to cellular Glc concentration, biosynthesis of *O*-GalNAc glycans in the nucleus may be significantly altered in situations involving changes in sugar metabolism, *e.g.* diabetes. Increased levels of *O*-GalNAc residues (*e.g.* Tn antigen) are often observed in epithelial cancer cells and likely may reflect changes in nuclear *O*-GalNAc glycan abundance. Diabetes and epithelial cancer are both associated with widespread changes in gene expression, which likely involve *O*-GalNAc glycans. PTMs of nuclear proteins play key roles in many nuclear physiological processes. It is therefore important to further elucidate the functions of *O*-GalNAc glycans in nuclear proteins. This is the focus of our ongoing studies.

Experimental procedures

Cell lines

Human cervical cancer (HeLa), human breast adenocarcinoma (MCF7), human breast tumor (T47D), human neuroblastoma (SK-N-AS), human kidney (HEK-293), human lung (MRC-5), monkey kidney (Vero) cell lines, Chinese hamster ovary (CHO) mutant cell line ldlD, and insect Sf9 cells were from CIQUIBIC-CONICET/Department of Biological Chemistry, Universidad Nacional de Córdoba, Argentina. Human, hamster, and monkey cell lines were grown at 37 °C in an incubator (10% CO_2 atmosphere) in Dulbecco's modified Eagle's medium (Sigma) supplemented with 10% fetal calf serum, 1 mM sodium pyruvate, and nonessential amino acids. To study the initiation of *O*-GalNAc glycosylation, CHO ldlD cells were grown in complete media supplemented with 1.5 mM GalNAc (GalNAc+) or not GalNAc (GalNAc−) during 48 h (44). Insect cells were grown at 27 °C in Grace's insect medium (Sigma) containing 10% fetal calf serum. Human mononuclear cells (HMC) were obtained from blood (from F. J. I.) by centrifugation at 400 × *g* for 30 min at 25 °C with Histopaque-1077 (Sigma).

Nuclei and nucleoplasm purification

Nuclei and nucleoplasm were purified as described by Shechter *et al.* (15) with some modifications. In brief, cultured cells were trypsinized, harvested, and washed with PBS by centrifugation at 300 × *g* for 10 min at 4 °C. 1×10^7 cells were incubated with 1 ml of extraction buffer (10 mM HEPES, pH 7.9, 10 mM KCl, 1.5 mM $MgCl_2$, 0.34 M sucrose, 10% glycerol) containing 0.2% Nonidet P-40 and protease inhibitors for 10 min on ice, with occasional rotation for cell lysis. The sample was centrifuged at 6,500 × *g* for 5 min at 4 °; the supernatant (cytoplasm) was recovered, and the pellet (intact nuclei) was washed three times with 1 ml of extraction buffer (without Nonidet P-40). Purity of nuclei was evaluated by immunofluorescence confocal

microscopy using mouse anti-Golgin 97 and mouse anti-calreticulin antibody as membrane organelle markers and Alexa 488-labeled rabbit anti-mouse IgG antibody as secondary reagent. Nuclei were stained with PI.

To obtain soluble the nuclear fraction (nucleoplasm), purified nuclei as above were lysed by incubation with 400 μl of high-salt solubilization buffer (50 mM Tris-HCl, pH 8.0, 2.5 M NaCl, 0.05% Nonidet P-40) for 20 min at 4 °C and then sonicated. The sample was centrifuged at 16,000 × *g* for 10 min at 4 °C, and supernatant (nucleoplasm) was recovered. A portion of each fraction equivalent to 1.5×10^5 cells was subjected to 4–20% SDS-PAGE. Purity of nuclei and nucleoplasm was evaluated by Western blotting with organelle molecular markers. Samples were also analyzed by CBB staining as loading control.

Fluorescence microscopy

Cells were grown on glass coverslips, and purified nuclei were seeded on polylysine-coated coverslips. Purified nuclei and cells were fixed for 20 min in 2% paraformaldehyde in phosphate-buffered saline (PBS: 20 mM sodium phosphate, pH 7.4, 150 mM sodium chloride), washed with PBS, permeabilized with 0.1% Triton X-100 and 200 mM glycine in PBS for 2 min, and washed again with PBS. Samples were blocked in 3% bovine serum albumin (BSA) for 60 min at room temperature and then incubated with antibody or lectin in PBS, 1% BSA for 2 h at room temperature. Antibodies used were as follows: mouse anti-Golgin 97 (1:500; A-21270; ThermoFisher Scientific); mouse anti-calreticulin (1:1,000; 612137; BD Biosciences); rabbit anti-human ppGalNAc-T3 (1:500; HPA007613; Sigma); and rabbit anti-human ppGalNAc-T2 (1:500; HPA011222; Sigma). Samples were washed with PBS and stained with Alexa 488- or 546-conjugated anti-rabbit or anti-mouse IgG (1:1,000; Invitrogen) for 1 h at room temperature.

For glycan detection, fixed, permeabilized, and blocked cells or nuclei were incubated with biotinylated lectins: *H. pomatia* agglutinin (biotin–HPA; 1:1,000; L6512; Sigma); *V. villosa* lectin (biotin–VVL; 1:2,500; B-1235; Vector Laboratories); or wheat germ agglutinin (biotin–WGA; 1:500; B-1025, Vector Laboratories) for 2 h at room temperature. Monoclonal IgM anti-Tn antibody (5F4) was incubated overnight at 4 °C, washed, and then incubated with biotinylated goat anti-mouse IgM antibody (1:1,000, BA-2020, Vector Laboratories) in PBS, 1% BSA for 2 h at room temperature. Samples were washed and stained for 1 h at room temperature with Alexa 488–streptavidin (1:2,000; 532354; Life Technologies, Inc.). Controls for immunostaining specificity were included with Alexa-conjugated anti-rabbit or -mouse IgG antibody or Alexa–streptavidin, but without primary antibody or biotinylated lectin. Nuclei were stained with DAPI and PI. Samples were mounted onto glass slides using FluorSave (Calbiochem). Images of ppGalNAc-T2 (T2) and ppGalNAc-T3 (T3) in the four human cell lines were obtained with a fluorescence microscope (Carl Zeiss, Axioplan) using PlanApoN 60 × 1.42 NA oil immersion objective. Images showing subcellular distribution of T3 and *O*-GalNAc glycosylation were obtained with a confocal microscope (model FV-1000, Olympus) using PlanApoN objective. Confocal images were acquired in sequential mode to avoid bleed-through between channels. Images were obtained in *x, y* and *x, y, z* scan modes. For zoomed images, region mode clip was performed, and stacks of equidistant (0.10 or 0.17 μm) planes were acquired. Zoom was adjusted to achieve 0.045 μm per pixel. Images were processed using the Fiji software program (45).

Western blotting (WB)

Protein samples were analyzed by SDS-PAGE as described previously (46). For protein antigens, electrotransferred membranes were blocked with 5% skim milk in PBS for 60 min at room temperature and incubated with appropriate primary antibodies overnight at 4 °C. The antibodies used (see details for some antibodies under "Fluorescence microscopy") were mouse anti-α-tubulin (1:2,500; clone DM1A, T9026; Sigma), mouse anti-Golgin 97 (1:100), mouse anti-calreticulin, and rabbit anti-histone H3 (1:5,000; AS10 710; Agrisera). Membranes were washed with PBS, incubated with IRDye 800-conjugated goat anti-rabbit or goat anti-mouse IgG antibody (1:20,000; LI-COR Biosciences) for 1 h at room temperature, washed again, and analyzed with an Odyssey IR Imaging System (LI-COR). For glycoprotein analysis, membranes were blocked with 3% polyvinylpyrrolidone (PVP) in PBS for 60 min at room temperature, incubated with biotin–HPA (1:1,000; Sigma), biotin–VVL (1:2,000; Vector Laboratories), or biotin–WGA (1:500; Vector Laboratories) for 2 h at room temperature, and then washed and incubated with IR800 dye-labeled streptavidin (1:30,000; LI-COR) in 0.3% PVP in PBS for 30 min at room temperature. Glycoproteins transferred to membrane were analyzed by IR imaging as above.

Expression and purification of recombinant human ppGalNAc-Ts

Human soluble ppGalNAc-T2 (T2) and ppGalNAc-T3 (T3) cDNAs were cloned into baculovirus expression vector pAcGP67 as described previously (47). Secreted, soluble proteins were purified from supernatant of Sf9 cell culture medium following centrifugation at 2,000 × *g* for 30 min at 4 °C. The supernatant was dialyzed (membrane MWCO <10 kDa) against PBS and centrifuged at 2,500 × *g* for 30 min at 4 °C. Proteins were purified using HisPur™ cobalt resin (ThermoFisher Scientific), eluted with 150 mM imidazole, dialyzed three times against PBS, and concentrated by a centrifuge filter device (MWCO <10 kDa; Millipore). Total proteins were measured by bicinchoninic acid assay with BSA as standard (Pierce; ThermoFisher Scientific). Purity of recombinant human ppGalNAc-Ts was assessed by 10% SDS-PAGE and CBB staining.

UDP-GalNAc measurement

UDP-GalNAc was measured by enzymatic assay. Microtiter plates were adsorbed with 2 μg/ml MUC1 peptide in coating buffer overnight at 4 °C, washed with PBS, and blocked with PBS with 0.1% Tween 20 for 1 h at room temperature. Catalytic reaction mixture containing 25 mM sodium cacodylate, pH 7.4, 10 mM $MnCl_2$, 0.05% Tween 20, and 10 nM purified T2 in a total volume of 45 μl was incubated with either 5 μl of HeLa cytoplasm, last nuclear wash before obtaining nucleoplasm, or nucleoplasm for 15 min at 37 °C. Additional multiwell plates adsorbed with 2 μg/ml MUC1 were incubated with catalytic

reaction mixture and various concentrations of UDP-GalNAc (Sigma) as standard, for construction of a reference curve. After catalytic reactions, plates were washed with PBS, incubated with biotin–VVL (1:1,000) in PBS with 0.05% Tween 20 for 60 min at room temperature, washed again with PBS, incubated with HRP–streptavidin (1:2,500) in PBS with 0.05% Tween 20 for 30 min at room temperature, and washed again with PBS. Peroxidase colorimetric reaction and absorbance reading were as described above.

To evaluate the capacity of UDP-GalNAc to enter the nucleus, 50 μl of purified nuclei were incubated with 50 μl of UDP-GalNAc (500 μM) in TBS for 10 min on ice, and washed three times with 1 ml extraction of buffer (10 mM HEPES, pH 7.9, 10 mM KCl, 1.5 mM $MgCl_2$, 0.34 M sucrose, 10% glycerol) by centrifugation at 6,500 $\times$ *g* for 5 min at 4 °C. Purified nuclei were sonicated, and the supernatant (nucleoplasm) was obtained by centrifugation at 16,000 $\times$ *g* for 10 min at 4 °C. UDP-GalNAc was measured in samples corresponding to the last nuclear wash and nucleoplasm.

Specificity of HPA, VVL, and WGA lectins

Lectin specificities were analyzed as described previously (48). Polystyrene microtiter plates (Corning, Costar) were coated with various concentrations of peptide $MUC1_{60}$ (TAPPAHGVTSAPDTRPAPGSTAPPAHGVTSAPDTRPAPGSTAPPAHGVTSAPDTRPAPGS) (MUC1), glycopeptide $MUC1_{60}\alpha GalNAc_{15}$ (MUC1αGalNAc), BSA, or ovalbumin in 0.1 sodium carbonate, pH 9.6, 0.5 M NaCl (coating buffer) overnight at 4 °C, washed with PBS, and blocked with 0.1% Tween 20 in PBS for 1 h at room temperature. Naked (MUC1 and BSA) and glycosylated proteins (MUC1αGalNAc and ovalbumin) were incubated with biotin–VVL (1:1,000), biotin–HPA (1:1,000), or biotin–WGA (1:600) in PBS with 0.05% Tween 20 for 60 min at room temperature. Multiwell plates were washed with PBS, incubated 30 min at room temperature with HRP–streptavidin (1:2,500; DakoCytomation) in PBS with 0.05% Tween 20, and washed with PBS. Colorimetric reaction was developed with 0.5 mg/ml *o*-phenylenediamine and 0.02% H_2O_2 in 100 mM sodium citrate, pH 5.0, for 15 min at room temperature, and the reaction was stopped by addition of 0.5 N H_2SO_4. Absorbance was read by microplate reader at 490 nm.

ppGalNAc-T activity

Microtiter plates were adsorbed with 2 μg/ml $MUC1_{24}$ (TAPPAHGVTSAPDTRPAPGSTAPP) or $MUC2_{33}$ (PTTTPITTTTTVTPTPTPTGTQTPTTTPISTTC) in coating buffer overnight at 4 °C, washed with PBS, and blocked with PBS with 0.1% Tween 20 for 1 h at room temperature. Catalytic reaction mixture (45 μl) containing 25 mM sodium cacodylate, pH 7.4, 10 mM $MnCl_2$, 0.05% Tween 20, and 100 μM UDP-GalNAc was incubated with either 5 μl of cytoplasm, last nuclear wash, or nucleoplasm for 15 min at 37 °C. The product, MUCαGalNAc, was detected with biotin–VVL as described above (49). Each sample was analyzed in triplicate.

For construction of the standard curve, microtiter plates were adsorbed with various concentrations of MUC1αGalNAc in coating buffer overnight at 4 °C, washed with PBS, and blocked with PBS with 0.1% Tween 20 for 1 h at room temperature. αGalNAc residues were detected using biotin–VVL as described in above. GalNAc-T activity was expressed as international units (1 unit = 1 μmol of α-linked GalNAc/min) and normalized relative to total proteins (units/mg).

O-GalNAc glycosylation in purified nuclei

Purified nuclei were divided into three equal samples and incubated with equal volumes of TBS with either 10 mM $MnCl_2$ (endogenous glycosylation), TBS with 10 mM $MnCl_2$ and 500 μM UDP-GalNAc (*O*-GalNAc over–glycosylated nuclei; "OG nuclei"), or TBS with 10 mM $MnCl_2$, and 500 μM UDP-GlcNAc (control) for 1 h at 37 °C. Nuclei were then washed three times with TBS, and the resulting purified nuclei were analyzed by fluorescence microscopy and WB. For fluorescence microscopy studies, treated nuclei were seeded on polylysine-coated coverslips, fixed, blocked, permeabilized, and incubated with biotinylated lectins (HPA and VVL) or monoclonal IgM anti-Tn antibody (5F4) to reveal αGalNAc residues. Nuclei were stained with PI and imaged by confocal microscopy (model FV-1000, Olympus) in *x, y* and *x, y, z* scan modes. Region mode clip was performed, and stacks of 20–30 equidistant (0.17 μm) planes were acquired. Zoom was adjusted to achieve 0.045 μm per pixel. Images were acquired using identical settings of laser power, detector gain, and offset.

HeLa cells, cytoplasm, purified nuclei, purified nuclei preincubated with UDP-GalNAc (OG nuclei), and purified nuclei preincubated with UDP-GlcNAc (control) were analyzed by WB using biotin–VVL and biotin–WGA. A portion of each fraction equivalent to 1.5 $\times$ 10^5 cells was subjected to 4–20% SDS-PAGE and CBB-stained or electrotransferred to nitrocellulose membranes. *O*-GalNAc and *O*-GlcNAc glycoproteins were detected, respectively, with biotin–VVL and biotin–WGA. Purified OG nuclei were sonicated, incubated without or with chicken liver α-*N*-acetylgalactosaminidase (A9763; Sigma) in 100 mM sodium citrate, pH 5.5, for 2 h at 37 °C, and analyzed by SDS-PAGE (12% acrylamide) and WB with biotin–HPA detection.

Quantification of nuclear O-GalNAc glycosylation

Purified nuclei and OG nuclei were processed for fluorescence microscopy, stained with Alexa 488–streptavidin (negative control: without lectin) or with biotin–VVL followed by Alexa 488–streptavidin, and finally stained with PI. Samples were imaged in *x, y, z* scan mode, and stacks of 3–4 equidistant (0.7 μm) planes were obtained. Images were acquired with identical settings of laser power, detector gain, and offset. Z-stack images were processed by Fiji program. Signal in the 488 channel (corresponding to *O*-GalNAc glycosylation detected with VVL and nonspecific signal in negative controls) was measured. The *z* axis profile and selection of the nuclear plane (546 channel) (PI) were performed for each stack. A nuclear mask created by nuclear signal thresholding (546 channel) (Huang method) was used to determine mean intensity in the 488 channel for each nucleus, under each condition. Background was pre-subtracted for both channels.

CHO ldlD cells grown in coverslips were processed for fluorescence microscopy in the same way that purified nuclei, and

the cell nucleus was stained with DAPI. Images of cells were acquired with identical settings and were processed in the same way using Fiji software. To measure the signal in the nuclear region, nuclear masks were generated by DAPI nuclear signal thresholding. Background was subtracted, and the mean fluorescence in the nuclear region corresponding to nuclear terminal *O*-GalNAc was measured in 58–60 individual cells for each condition (+GalNAc/−GalNAc). The resulting fluorescence values were relativized to the average fluorescence in the −GalNAc condition (the condition with lower *O*-GalNAc glycosylation), and finally, measurements were expressed as relative nuclear mean fluorescence. All data were analyzed using the GraphPad Prism 5 software program.

Specificity of rabbit anti-human T3 antibody

Purified human T3 (1 μg) or HeLa homogenate (40 μg) was loaded onto 10% SDS-PAGE, electrotransferred, and analyzed by WB using rabbit anti-human T3 antibody and IRDye 800-conjugated goat anti-rabbit IgG antibody (1:20,000). Specificity of T3 (72 kDa) recognition was analyzed based on the molecular weight of recognized protein.

Specificity of the anti-human T3 antibody was evaluated by competitive immunofluorescence assay. HeLa cells were grown on coverslips and subjected to immunofluorescence microscopy. Fixed, permeabilized, and blocked cells were incubated for 2 h at room temperature with anti-human T3 antibody (1:500) either alone (control) or with purified human T3 (0.9 μg/ml). Coverslips were washed and incubated with Alexa 546-conjugated anti-rabbit IgG antibody (1:1,000), and nuclei were stained with DAPI. Samples were imaged as described under "Fluorescence microscopy," using identical settings of laser power, detector gain, and offset.

Identification of O-GalNAc–glycosylated proteins

O-GalNAc glycoproteins from HeLa nucleoplasm (endogenous glycosylation) and nucleoplasm from OG nuclei were purified by affinity chromatography using VVL–biotin/streptavidin–agarose column (+VVL column). +VVL column was prepared by incubation of 100 μg of biotin–VVL with 100 μl of streptavidin–agarose CL-4B (85881; Sigma) for 1 h at 4 °C, washed with 10 volumes TBS, and divided into two 50-μl parts. To obtain nucleoplasm, 2×10^7 HeLa-purified nuclei or OG nuclei (preincubated with UDP-GalNAc for 1 h at 37 °C) were lysed in high-salt solubilization buffer as described previously (15). Each nucleoplasm was pre-adsorbed with 50 μl of streptavidin–agarose column for 1 h at 4 °C. Resulting nucleoplasms were divided into two equal parts, which were incubated, respectively, with 50 μl of VVL-biotin/streptavidin–agarose column (+VVL column) and with 50 μl of streptavidin–agarose column without VVL (−VVL column) for 1 h at 4 °C. Columns were washed with 20 volumes of TBS, resuspended in Laemmli sample buffer, and heated at 90 °C for 10 min. Samples were loaded onto SDS-PAGE (12% acrylamide), run until 1-cm front separation, and gel stained with colloidal CBB G (B1131; Sigma). Gel regions corresponding to +VVL and −VVL columns were analyzed at a MS facility (Centro de Estudios Químicos y Biológicos por Espectrometría de Masa, Universidad de Buenos Aires, Argentina). Samples were digested with trypsin, and peptides were purified by nano-LC-MS/MS in a Q-Exactive mass spectrometer (ThermoFisher Scientific). A H_2O/acetonitrile gradient at a flow rate of 33 nl/min was used with a C18 2-mm EASY-Spray Accucore (ES801; ThermoFisher Scientific) coupled to Q-Exactive–Orbitrap hybrid spectrometer (ThermoFisher Scientific). The top 12 peaks in each cycle were fragmented by the data-dependent MS2 method. Data analysis was performed using the Proteome Discoverer software program, version 1.4. Based on the results, the following criterion was established. Proteins were considered *O*-GalNAc– glycosylated for those hits in the +VVL column having $\geq$ 2 high-quality peptides and peptide spectrum matches ratio (PSM ratio) of $\geq$3. PSM ratio was calculated as PSM for a hit identified in the +VVL column divided by PSM of the same hit in the −VVL column. Thus, the criterion was PSM ratio (+VVL column PSM/−VVL column PSM) of $\geq$3.

Prediction of LMNB1 O-GalNAc glycosylation

The LMNB1 amino acid sequence (UniProtKB-P20700 LMNB1_HUMAN) was analyzed for *O*-GalNAc glycosylation site prediction using the bioinformatic NetOGlyc 4.0 server (cbs.dtu.dk/services/NetOGlyc/).[4]

O-GalNAc over-glycosylation of nuclei expressing LMNB1

HeLa cells (80% confluence) were transfected for 2 h using Lipofectamine Transfection Reagent (ThermoFisher Scientific) with mCherry–LMNB1–10 plasmid (55069; Addgene). Transfected cells were incubated for 24 h at 37 °C, harvested, and subjected to subcellular fractionation for nuclei purification. Purified nuclei were incubated without or with UDP-GalNAc in glycosylation buffer for 1 h at 37 °C as described above, washed with PBS, seeded onto polylysine-coated coverslips, and subjected to fluorescence microscopy.

O-GalNAc/LMNB1 correlation analysis

HeLa-purified nuclei and OG nuclei expressing Cherry–LMNB1 were stained with biotin–VVL (1:1,000) or biotin–WGA (1:500) (control) and then with Alexa 488–streptavidin (1:2,000). Samples were imaged by confocal microscopy (model FV-1200, Olympus) using PlanApoN objective. Images were acquired in constant acquisition settings and sequential mode to avoid bleed-through between channels and processed using the Fiji program. Background was subtracted; a Gaussian filter with $\sigma = 2$ was applied, and correlation analysis of green (Alexa 488/channel 1) and red (cherry/channel 2) channels was performed. Intensity profiles of the two channels were obtained using BAR extension 1.1.6. Fluorograms and Pearson's correlation coefficients were obtained by the JaCoP extension, using Costes' automated thresholding method.

Acceptor photobleaching/FRET assay

HeLa nuclei and OG nuclei were treated as indicated above. FRET assay was performed using a confocal microscope (model FV-1200, Olympus) with PlanApoN objective. Images were acquired in constant acquisition settings and sequential mode before and after bleaching. Samples were subjected to bleaching for 2 ms in the acceptor channel (Cherry–LMNB1) receiving complete photobleaching. The area of bleaching region was

constant. Change of fluorescence in donor channel (Alexa 488) was evaluated after acceptor photobleaching, and FRET index for each pixel was calculated as shown in Equation 1,

$$\text{FRET index} = 1 - \frac{\text{donor fluorescence in presence of acceptor}}{\text{donor fluorescence in absence of acceptor}} \quad \text{(Eq. 1)}$$

Mean FRET index ($n = 5$) in the bleaching area was quantified for each condition. Images were processed using Fiji and FV10-ASW 3.1 software programs.

Statistical analysis

Means were compared by Mann-Whitney test or unpaired *t* test, using GraphPad Prism 5. Standard error of the mean (S.E.) is shown as error bars in figures. Statistical significance of differences between means is indicated by * ($p < 0.05$); ** ($p < 0.01$); *** ($p < 0.001$), or *ns* (not significant).

Author contributions—R. B. C., V. L., and Y. C. G. formal analysis; R. B. C., V. L., Y. C. G., and F. J. I. investigation; R. B. C., V. L., and Y. C. G. methodology; F. J. I. supervision; F. J. I. funding acquisition; F. J. I. writing-original draft; F. J. I. project administration.

Acknowledgments—We are grateful to S. Deza and G. Schachner for cell culture assistance, Drs. C. Mas and C. Sampedro for confocal microscopy assistance, and Dr. S. Anderson for English editing of the manuscript.

References

1. Skalska, L., Beltran-Nebot, M., Ule, J., and Jenner, R. G. (2017) Regulatory feedback from nascent RNA to chromatin and transcription. *Nat. Rev. Mol. Cell Biol.* **18,** 331–337 CrossRef Medline
2. Drickamer, K., and Taylor, M. E. (2015) Recent insights into structures and functions of C-type lectins in the immune system. *Curr. Opin. Struct. Biol.* **34,** 26–34 CrossRef Medline
3. Lloyd, J. T., and Glass, K. C. (2018) Biological function and histone recognition of family IV bromodomain-containing proteins. *J. Cell. Physiol.* **233,** 1877–1886 CrossRef Medline
4. Hart, G. W., Housley, M. P., and Slawson, C. (2007) Cycling of *O*-linked β-*N*-acetylglucosamine on nucleocytoplasmic proteins. *Nature* **446,** 1017–1022 CrossRef Medline
5. Love, D. C., Kochan, J., Cathey, R. L., Shin, S. H., Hanover, J. A., and Kochran, J. (2003) Mitochondrial and nucleocytoplasmic targeting of *O*-linked GlcNAc transferase. *J. Cell Sci.* **116,** 647–654 CrossRef Medline
6. Gambetta, M. C., and Müller, J. (2015) A critical perspective of the diverse roles of *O*-GlcNAc transferase in chromatin. *Chromosoma* **124,** 429–442 CrossRef Medline
7. Hanover, J. A., Krause, M. W., and Love, D. C. (2012) Bitterrsweet memories: linking metabolism to epigenetics through *O*-GlcNAcylation. *Nat. Rev. Mol. Cell Biol.* **13,** 312–321 CrossRef Medline
8. Banerjee, P. S., Lagerlöf, O., and Hart, G. W. (2016) Roles of *O*-GlcNAc in chronic diseases of aging. *Mol. Aspects Med.* **51,** 1–15 CrossRef Medline
9. Wollaston-Hayden, E. E., Harris, R. B., Liu, B., Bridger, R., Xu, Y., and Wells, L. (2015) Global O-GlcNAc levels modulate transcription of the adipocyte secretome during chronic insulin resistance. *Front. Endocrinol.* **5,** 223 CrossRef Medline
10. Bennett, E. P., Mandel, U., Clausen, H., Gerken, T. A., Fritz, T. A., and Tabak, L. A. (2012) Control of mucin-type *O*-glycosylation: a classification of the polypeptide GalNAc-transferase gene family. *Glycobiology* **22,** 736–756 CrossRef Medline
11. Nilsson, T., Au, C. E., and Bergeron, J. J. (2009) Sorting out glycosylation enzymes in the Golgi apparatus. *FEBS Lett.* **583,** 3764–3769 CrossRef Medline
12. Kumar, S. R., Sauter, E. R., Quinn, T. P., and Deutscher, S. L. (2005) Thomsen-Friedenreich and Tn antigens in nipple fluid: carbohydrate biomarkers for breast cancer detection. *Clin. Cancer Res.* **11,** 6868–6871 CrossRef Medline
13. Brockhausen, I. (2006) Mucin-type *O*-glycans in human colon and breast cancer: glycodynamics and functions. *EMBO Rep.* **7,** 599–604 CrossRef Medline
14. Yu, L. G., Andrews, N., Zhao, Q., McKean, D., Williams, J. F., Connor, L. J., Gerasimenko, O. V., Hilkens, J., Hirabayashi, J., Kasai, K., and Rhodes, J. M. (2007) Galectin-3 interaction with Thomsen-Friedenreich disaccharide on cancer-associated MUC1 causes increased cancer cell endothelial adhesion. *J. Biol. Chem.* **282,** 773–781 CrossRef Medline
15. Shechter, D., Dormann, H. L., Allis, C. D., and Hake, S. B. (2007) Extraction, purification and analysis of histones. *Nat. Protoc.* **2,** 1445–14457 CrossRef Medline
16. Varki, A., Esko, J. D., and Colley, K. J. (2009) in *Essentials of Glycobiology* (Varki, A., Cummings, R. D., Esko, J. D., Freeze, H. H., Stanley, P., Bertozzi, C. R., Hart, G. W., and Etzler, M. E., eds) pp. 37–46, Cold Spring Harbor Laboratory Press, Cold Spring Harbor, NY
17. Gill, D. J., Tham, K. M., Chia, J., Wang, S. C., Steentoft, C., Clausen, H., Bard-Chapeau, E. A., and Bard, F. A. (2013) Initiation of GalNAc-type *O*-glycosylation in the endoplasmic reticulum promotes cancer cell invasiveness. *Proc. Natl. Acad. Sci. U.S.A.* **110,** E3152–E3161 CrossRef Medline
18. Steentoft, C., Vakhrushev, S. Y., Joshi, H. J., Kong, Y., Vester-Christensen, M. B., Schjoldager, K. T., Lavrsen, K., Dabelsteen, S., Pedersen, N. B., Marcos-Silva, L., Gupta, R., Bennett, E. P., Mandel, U., Brunak, S., Wandall, H. H., *et al.* (2013) Precision mapping of the human *O*-GalNAc glycoproteome through SimpleCell technology. *EMBO J.* **32,** 1478–1488 CrossRef Medline
19. Prokocimer, M., Davidovich, M., Nissim-Rafinia, M., Wiesel-Motiuk, N., Bar, D. Z., Barkan, R., Meshorer, E., and Gruenbaum, Y. (2009) Nuclear lamins: key regulators of nuclear structure and activities. *J. Cell. Mol. Med.* **13,** 1059–1085 CrossRef Medline
20. Zhu, Y., Liu, T. W., Madden, Z., Yuzwa, S. A., Murray, K., Cecioni, S., Zachara, N., and Vocadlo, D. J. (2016) Post-translational *O*-GlcNAcylation is essential for nuclear pore integrity and maintenance of the pore selectivity filter. *J. Mol. Cell. Biol.* **8,** 2–16 CrossRef Medline
21. Hart, G. W., and Akimoto, Y. (2009) in *Essentials of Glycobiology* (Varki, A., Cummings, R. D., Esko, J. D., Freeze, H. H., Stanley, P., Bertozzi, C. R., Hart, G. W., and Etzler, M. E., eds) pp. 263–279, Cold Spring Harbor Laboratory Press, Cold Spring Harbor, NY
22. Bond, M. R., and Hanover, J. A. (2015) A little sugar goes a long way: the cell biology of *O*-GlcNAc. *J. Cell Biol.* **208,** 869–880 CrossRef Medline
23. Vilcaes, A. A., Demichelis, V. T., and Daniotti, J. L. (2011) Trans-activity of plasma membrane-associated ganglioside sialyltransferase in mammalian cells. *J. Biol. Chem.* **286,** 31437–31446 CrossRef Medline
24. Trapannone, R., Mariappa, D., Ferenbach, A. T., and van Aalten, D. M. (2016) Nucleocytoplasmic human *O*-GlcNAc transferase is sufficient for *O*-GlcNAcylation of mitochondrial proteins. *Biochem. J.* **473,** 1693–1702 CrossRef Medline
25. Uhlen, M., Oksvold, P., Fagerberg, L., Lundberg, E., Jonasson, K., Forsberg, M., Zwahlen, M., Kampf, C., Wester, K., Hober, S., Wernerus, H., Björling, L., and Ponten, F. (2010) Towards a knowledge-based human protein Atlas. *Nat. Biotechnol.* **28,** 1248–1250 CrossRef Medline
26. Uhlén, M., Fagerberg, L., Hallström, B. M., Lindskog, C., Oksvold, P., Mardinoglu, A., Sivertsson, Å., Kampf, C., Sjöstedt, E., Asplund, A., Olsson, I., Edlund, K., Lundberg, E., Navani, S., Szigyarto, C. A., *et al.* (2015) Proteomics. Tissue-based map of the human proteome. *Science* **347,** 1260419 CrossRef Medline
27. Collas, P., Lund, E. G., and Oldenburg, A. R. (2014) Closing the (nuclear) envelope on the genome: how nuclear lamins interact with promoters and modulate gene expression. *Bioessays* **36,** 75–83 CrossRef Medline
28. Xie, W., and Burke, B. (2016) Lamins. *Curr. Biol.* **26,** R348–R350 CrossRef Medline

29. Fox, A. H., and Lamond, A. I. (2010) Paraspeckles. *Cold Spring Harb. Perspect. Biol.* **2,** a000687 Medline
30. Tschochner, H., and Hurt, E. (2003) Pre-ribosomes on the road from the nucleolus to the cytoplasm. *Trends Cell Biol.* **13,** 255–263 CrossRef Medline
31. Yadavilli, S., Hegde, V., and Deutsch, W. A. (2007) Translocation of human ribosomal protein S3 to sites of DNA damage is dependent on ERK-mediated phosphorylation following genotoxic stress. *DNA Repair* (*Amst.*) **6,** 1453–1462 CrossRef
32. Castello, A., Fischer, B., Eichelbaum, K., Horos, R., Beckmann, B. M., Strein, C., Davey, N. E., Humphreys, D. T., Preiss, T., Steinmetz, L. M., Krijgsveld, J., and Hentze, M. W. (2012) Insights into RNA biology from an atlas of mammalian mRNA-binding proteins. *Cell* **149,** 1393–1406 CrossRef Medline
33. Adamson, B., Smogorzewska, A., Sigoillot, F. D., King, R. W., and Elledge, S. J. (2012) A genome-wide homologous recombination screen identifies the RNA-binding protein RBMX as a component of the DNA-damage response. *Nat. Cell Biol.* **14,** 318–328 CrossRef Medline
34. Aktaş, T., Avşar Ilık İ., Maticzka, D., Bhardwaj, V., Pessoa Rodrigues, C., Mittler, G., Manke, T., Backofen, R., and Akhtar, A. (2017) DHX9 suppresses RNA processing defects originating from the Alu invasion of the human genome. *Nature* **544,** 115–119 CrossRef Medline
35. Dechat, T., Pfleghaar, K., Sengupta, K., Shimi, T., Shumaker, D. K., Solimando, L., and Goldman, R. D. (2008) Nuclear lamins: major factors in the structural organization and function of the nucleus and chromatin. *Genes Dev.* **22,** 832–853 CrossRef Medline
36. Amendola, M., and van Steensel, B. (2014) Mechanisms and dynamics of nuclear lamina-genome interactions. *Curr. Opin. Cell Biol.* **28,** 61–68 CrossRef Medline
37. Simon, D. N., Domaradzki, T., Hofmann, W. A., and Wilson, K. L. (2013) Lamin A tail modification by SUMO1 is disrupted by familial partial lipodystrophy-causing mutations. *Mol. Biol. Cell* **24,** 342–350 CrossRef Medline
38. Torvaldson, E., Kochin, V., and Eriksson, J. E. (2015) Phosphorylation of lamins determine their structural properties and signaling functions. *Nucleus* **6,** 166–171 CrossRef Medline
39. Snider, N. T., and Omary, M. B. (2014) Post-translational modifications of intermediate filament proteins: mechanisms and functions. *Nat. Rev. Mol. Cell Biol.* **15,** 163–177 CrossRef Medline
40. Wang, Z., Udeshi, N. D., O'Malley, M., Shabanowitz, J., Hunt, D. F., and Hart, G. W. (2010) Enrichment and site mapping of *O*-linked *N*-acetylglucosamine by a combination of chemical/enzymatic tagging, photochemical cleavage, and electron transfer dissociation mass spectrometry. *Mol. Cell. Proteomics* **9,** 153–160 CrossRef Medline
41. Yang, Z., Halim, A., Narimatsu, Y., Jitendra Joshi, H., Steentoft, C., Schjoldager, K. T., Alder Schulz, M., Sealover, N. R., Kayser, K. J., Paul Bennett, E., Levery, S. B., Vakhrushev, S. Y., and Clausen, H. (2014) The GalNAc-type *O*-glycoproteome of CHO cells characterized by the SimpleCell strategy. *Mol. Cell. Proteomics* **13,** 3224–3235 CrossRef Medline
42. Camps, J., Erdos, M. R., and Ried, T. (2015) The role of lamin B1 for the maintenance of nuclear structure and function. *Nucleus* **6,** 8–14 CrossRef Medline
43. Klymenko, T., Bloehdorn, J., Bahlo, J., Robrecht, S., Akylzhanova, G., Cox, K., Estenfelder, S., Wang, J., Edelmann, J., Strefford, J. C., Wojdacz, T. K., Fischer, K., Hallek, M., Stilgenbauer, S., Cragg, M., *et al.* (2018) Lamin B1 regulates somatic mutation and progression of B cell malignancies. *Leukemia* **32,** 364–375 CrossRef Medline
44. Kingsley, D. M., Kozarsky, K. F., Hobbie, L., and Krieger, M. (1986) Reversible defects in *O*-linked glycosylation and LDL receptor expression in a UDP-Gal/UDP-GalNAc 4-epimerase deficient mutant. *Cell* **44,** 749–759 CrossRef Medline
45. Schindelin, J., Arganda-Carreras, I., Frise, E., Kaynig, V., Longair, M., Pietzsch, T., Preibisch, S., Rueden, C., Saalfeld, S., Schmid, B., Tinevez, J. Y., White, D. J., Hartenstein, V., Eliceiri, K., Tomancak, P., and Cardona, A. (2012) "Fiji: an open-source platform for biological-image analysis." *Nat. Methods* **9,** 676–682 Medline
46. Irazoqui, F. J., Vozari-Hampe, M. M., Lardone, R. D., Villarreal, M. A., Sendra, V. G., Montich, G. G., Trindade, V. M., Clausen, H., and Nores, G. A. (2005) Fine carbohydrate recognition of *Euphorbia milii* lectin. *Biochem. Biophys. Res. Commun.* **336,** 14–21 CrossRef Medline
47. Bennett, E. P., Hassan, H., and Clausen, H. (1996) cDNA cloning and expression of a novel human UDP-*N*-acetyl-α-D-galactosamine. Polypeptide *N*-acetylgalactosaminyltransferase, GalNAc-t3. *J. Biol. Chem.* **271,** 17006–17012 CrossRef Medline
48. Irazoqui, F. J., Vides, M. A., and Nores, G. A. (1999) Structural requirements of carbohydrates to bind *Agaricus bisporus* lectin. *Glycobiology* **9,** 59–64 CrossRef Medline
49. Lorenz, V., Ditamo, Y., Cejas, R. B., Carrizo, M. E., Bennett, E. P., Clausen, H., Nores, G. A., and Irazoqui, F. J. (2016) Extrinsic functions of lectin domains in *O*-*N*-acetylgalactosamine glycan biosynthesis. *J. Biol. Chem.* **291,** 25339–25350 CrossRef Medline

Biosynthesis of *O*-*N*-acetylgalactosamine glycans in the human cell nucleus

Romina B. Cejas, Virginia Lorenz, Yohana C. Garay and Fernando J. Irazoqui

J. Biol. Chem. 2019, 294:2997-3011.
doi: 10.1074/jbc.RA118.005524 originally published online December 27, 2018